ELECTRONIC SUPPLEMENTARY INFORMATION

Ultrafast Sensitivity-Controlled and Specific Detection of Extracellular Vesicles Using Optical Force with Antibody-modified Microparticles in a Microflow System

Kana Fujiwara[a,b,c,#], Yumiko Takagi[a,b#], Mamoru Tamura[b,d], Mika Omura[b,e], Kenta Morimoto, [b,e] Ikuhiko Nakase[b,e,*], Shiho Tokonami[b,c,*], Takuya Iida[a,b,*]

[a]Department of Physics, Graduate School of Science, Osaka Metropolitan University, 1-2 Gakuen-cho, Naka-ku, Sakai, Osaka 599-8570, Japan.

[b]Research Institute for Light-induced Acceleration System (RILACS), Osaka Metropolitan University, 1-2 Gakuen-cho, Naka-ku, Sakai, Osaka 599-8570, Japan.

[c]Department of Applied Chemistry, Graduate School of Engineering, Osaka Metropolitan University, 1-2 Gakuen-cho, Naka-ku, Sakai, Osaka 599-8570, Japan.

[d]Department of Materials Engineering Science, Graduate School of Engineering Science, Osaka University, 1-3 Machikaneyama-cho, Toyonaka, Osaka 560-8531, Japan

[e]Department of Biological Chemistry, Graduate School of Science, Osaka Metropolitan University, 1-2 Gakuen-cho, Naka-ku, Sakai, Osaka 599-8570, Japan.

**Correspondence to: t-iida@omu.ac.jp (T.I.); tokonami@omu.ac.jp (S.T.); i-nakase@omu.ac.jp (I.N.)*

[#]These authors contributed equally to this work.

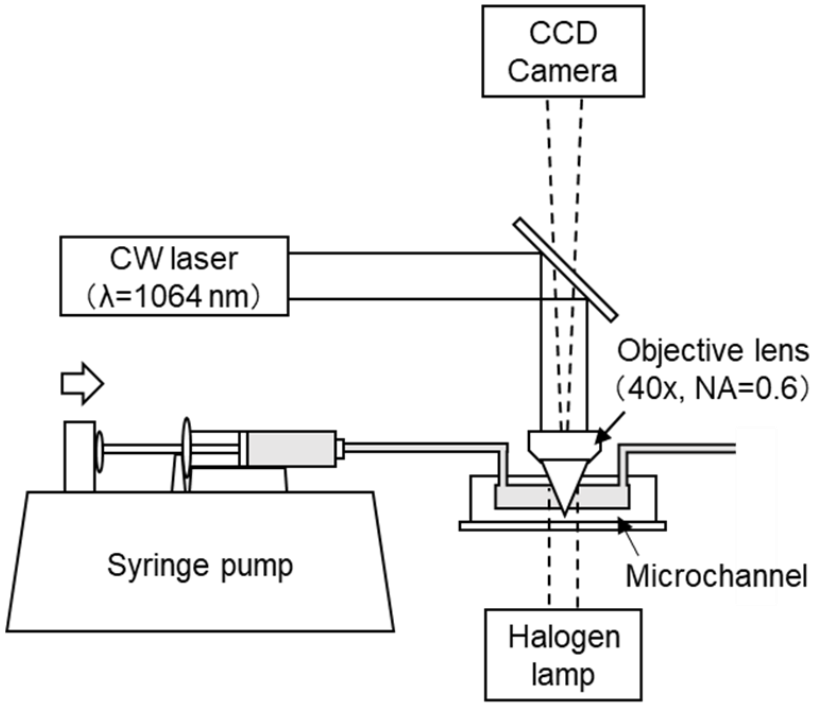

Figure S1. Microflow-type optical condensation system. Schematic diagram of the optical system used in this study.

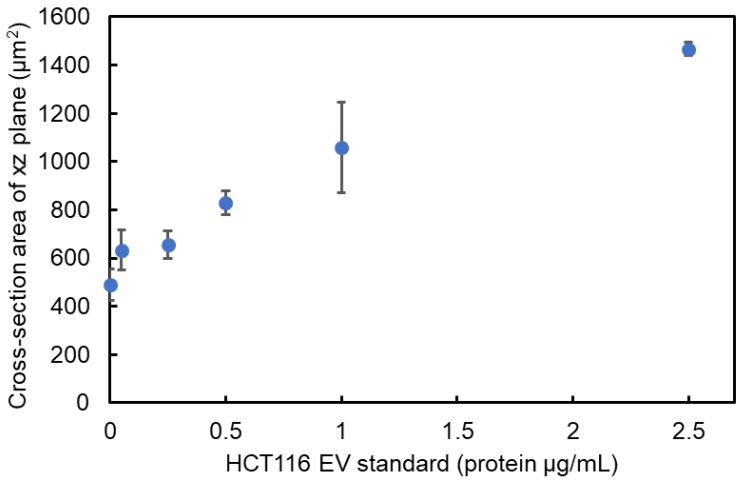

Figure S2. Calibration curve obtained by confocal imaging after the light-induced assembly. HCT116-derived nanoscale EV concentration dependence of xz-cross-section areas of the assembled structure in three-dimensional confocal images of Fig. 2b.

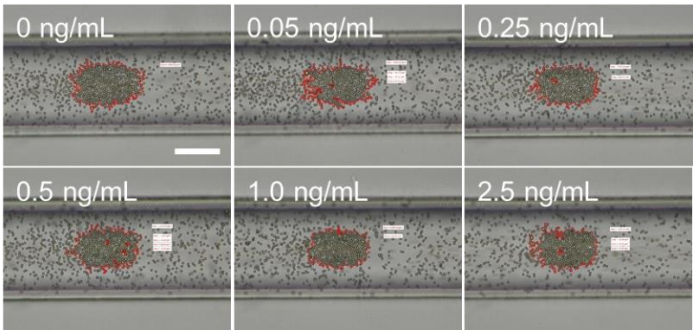

Figure S3. Transmission images of the negative control established using another type of protein. Transmission images of light-induced assembly without and with calnexin. Each concentration of calnexin is shown in the upper left section of the image, and the scale bar is 50 μm.

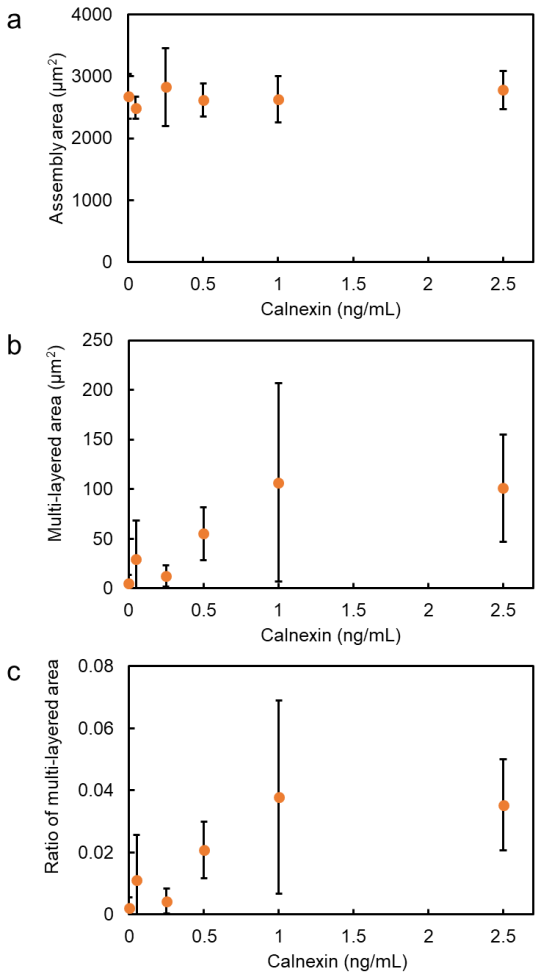

Figure S4. Concentration detection in the negative control established using another type of protein. Dependence of calnexin concentration on the (a) assembly area, (b) multi-layered area, and (c) ratio of the multi-layered area. Error bars present standard deviations (n = 3).

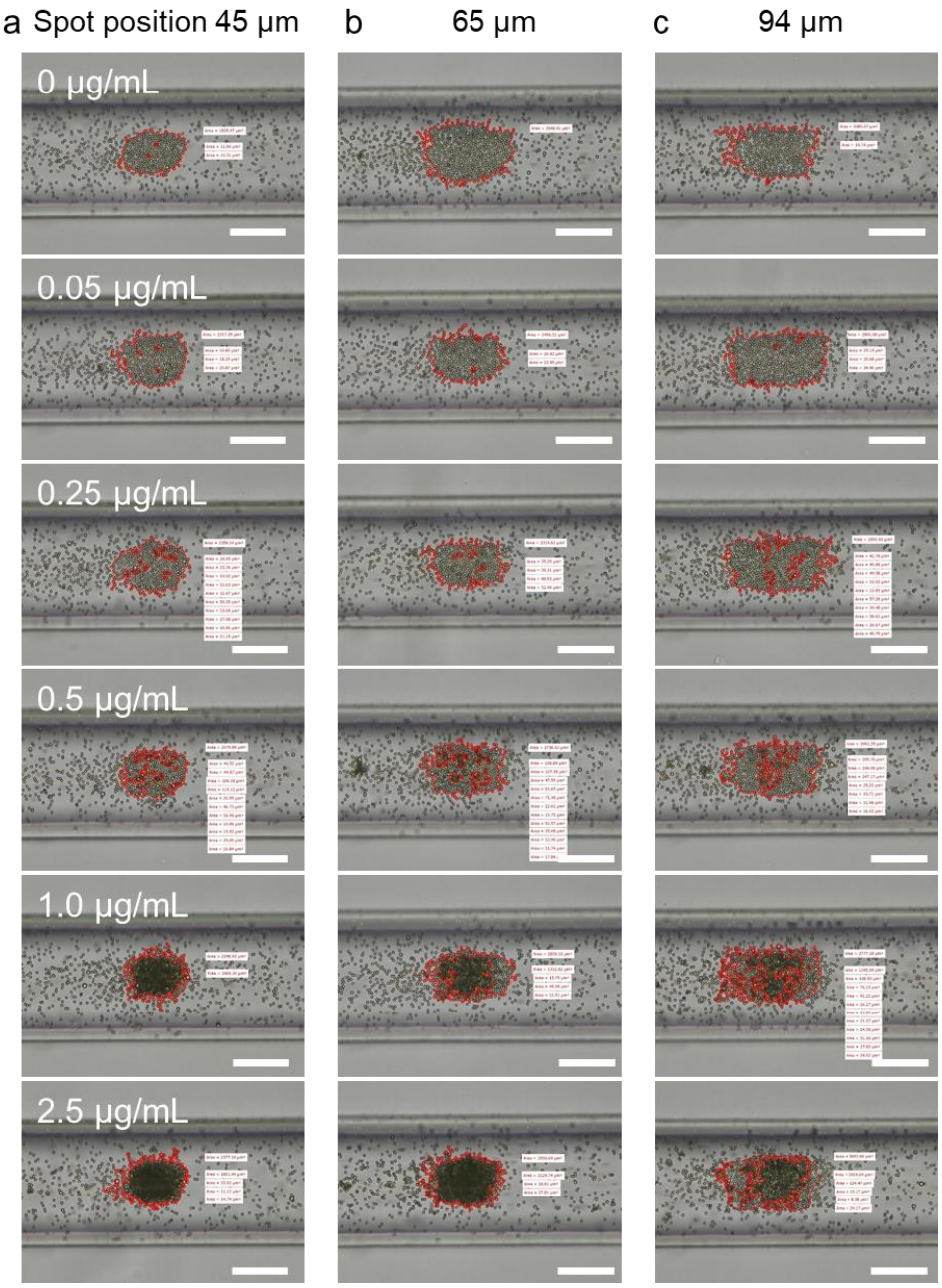

Figure S5. Light-induced assembly at different laser focusing distances. Transmission images of light-induced assembly with and without HCT116-derived nanoscale EVs at each focusing distance. (a–c) Images of assembled structures for focusing distance of 45 μm, 65 μm, and 94 μm, respectively, with various concentrations of nanoscale EVs. All scale bars are 50 μm.

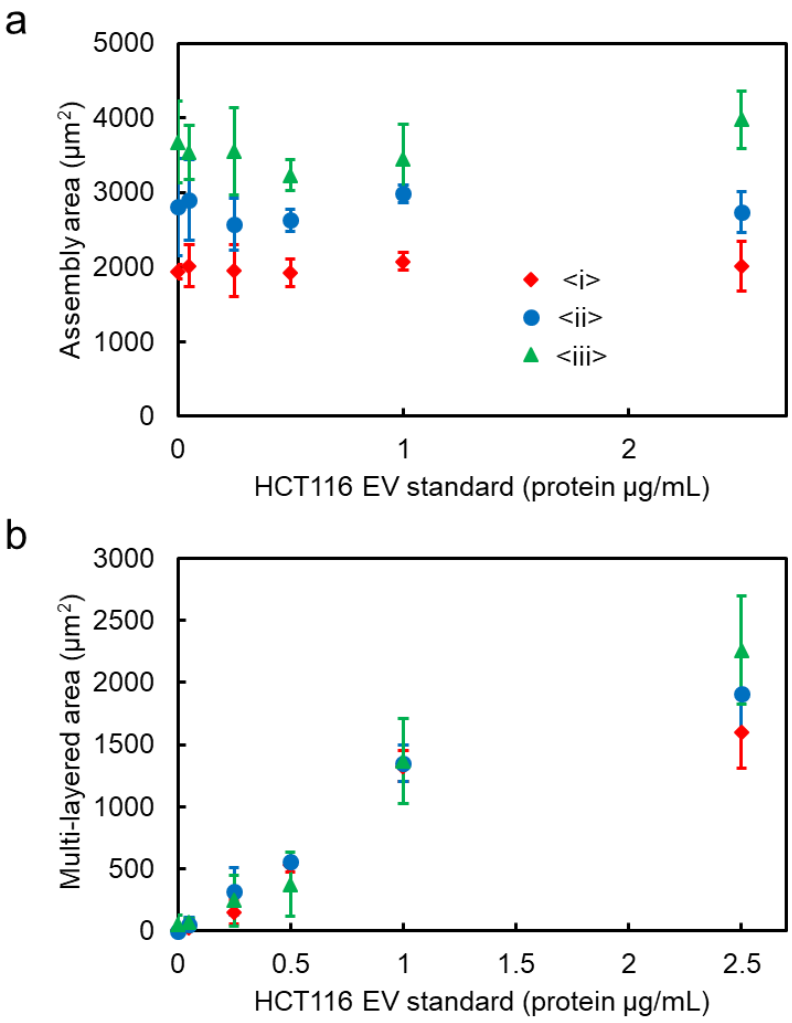

Figure S6. Size of the aggregate produced by light-induced assembly at different focusing distances. (a) The assembly area and (b) multi-layered area at each focusing distance are presented in Figure S5 (<i> FD = 45 μm, <ii> FD = 65 μm and <iii> FD = 94 μm in Figure 4a). Error bars present the standard deviations (n = 3) related to Figure 3 and Figure 4 in the main text.

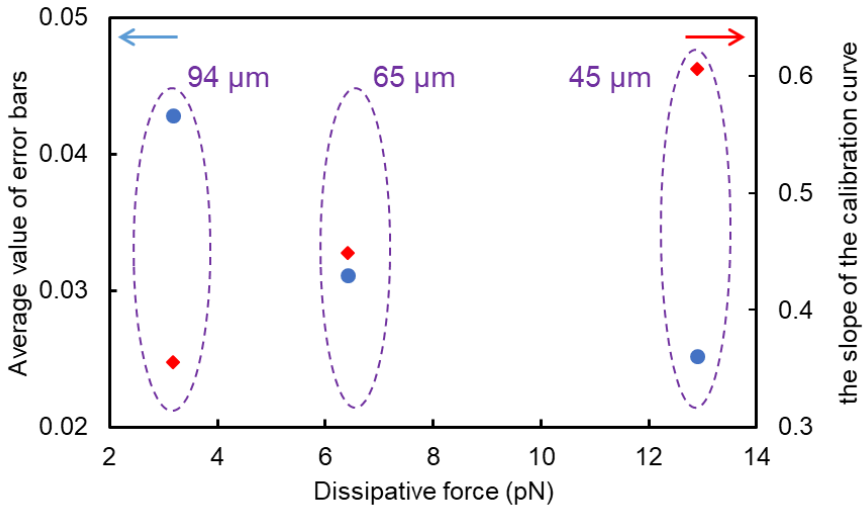

Figure S7. Evaluation of sensitivity by changing the optical pressure. Relation of the average value of error bars and the slope of the calibration curve (second vertical axis) in Figure 4b, depending on the dissipative force for a focusing distance (<i> FD = 45 µm, <ii> FD = 65 µm and <iii> FD = 94 µm in Figure 4a).

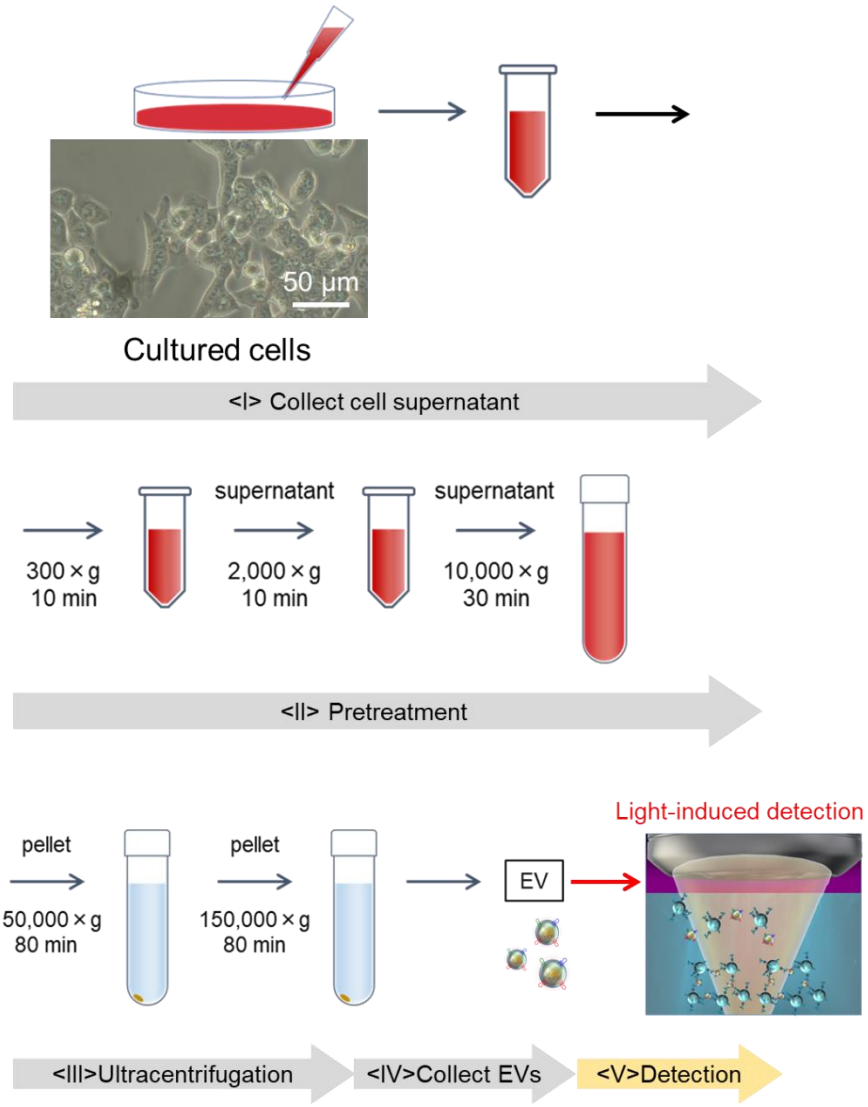

Figure S8. Schematic image of detection process of nanoscale EVs using the ultracentrifugation. Whole the process takes over 3.5 hours before the light-induced detection due to the complicated pretreatment processes.

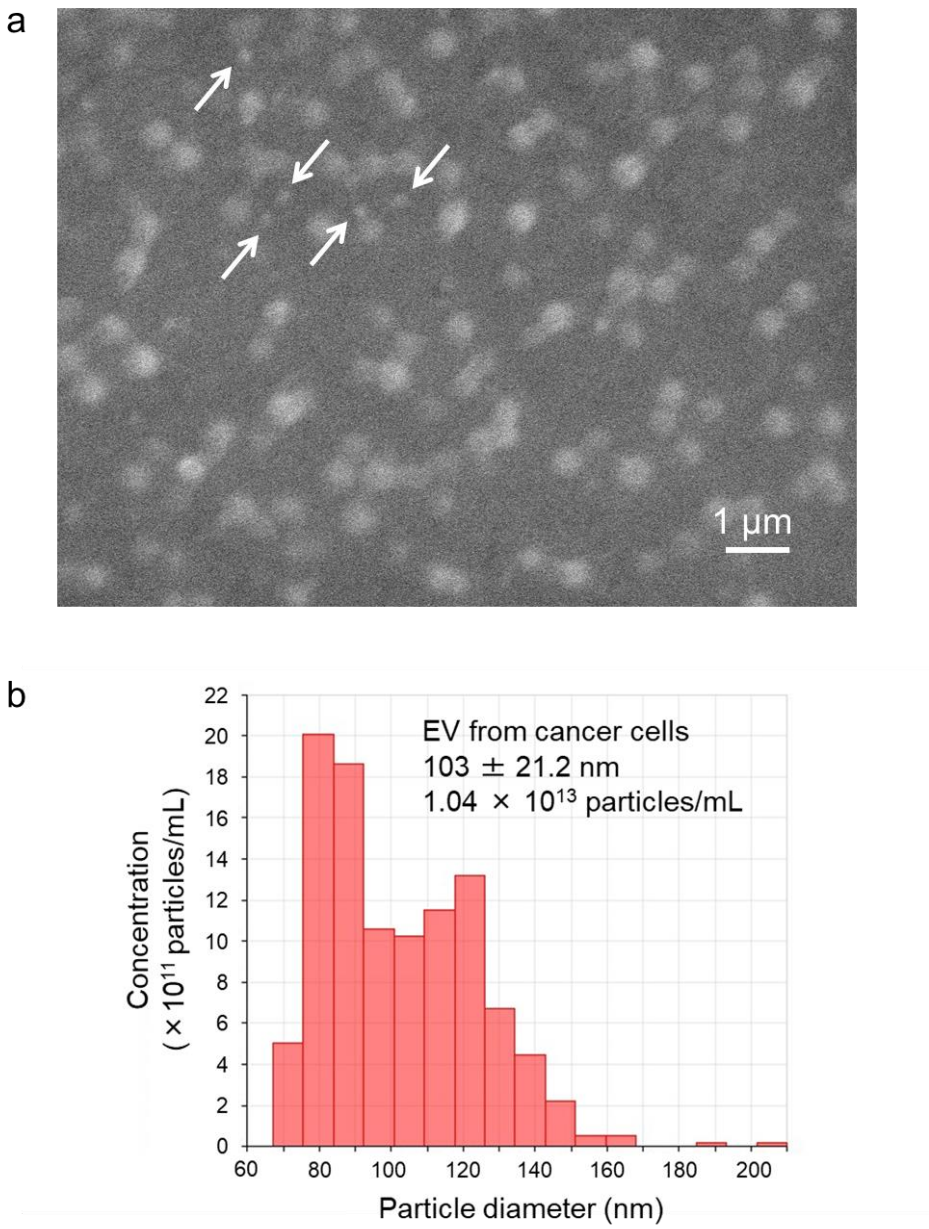

Figure S9. Scanning electron microscope (SEM) image and results of nanopore measurement of secreted substances in supernatant of cultured HCT116 cells. (a) Particles in the area between the centre of the droplet and the edge were observed by SEM at a magnification of X10000. Since salt crystals and other substances in the supernatant interfered with observation, the samples were dried after the solvent was replaced with deuterium-depleted water (DDW) for the SEM observation. (b) After the ultracentrifugation, size and concentration of collected EVs were evaluated with a nanoparticle analyser, qNano (IZON S/N 601A, Izon Science, New Zealand).

Movies for dynamics simulation of probe microparticles

Movie S1. Video of the theoretical result for light-induced assembly of microparticles using optical force in the microflow channel, where there is no interparticle binding force. Cohesion energy density: 0 J/m^3, volume flow rate: 0.05μL/min, laser power: 265 mW, focal point from the bottom of the microchannel FD: 45 μm. The laser was irradiated during the initial 3 s and was turned off subsequently. This video corresponds to Figure 5a.

Movie S2. Video of the theoretical result for the light-induced assembly of microparticles using optical pressure in the microflow channel, where the interparticle binding force is strong. Cohesion energy density: 100 J/m^3, volume flow rate: 0.05 μL/min, laser power: 265 mW, focal point from the bottom of the microchannel FD: 45 μm. The laser was irradiated during the initial 3 s and was turned off subsequently. This video corresponds to Figure 5d.

Movie S3. Video of the theoretical result for the light-induced assembly of microparticles using optical pressure in the microflow channel, where there is no interparticle binding force. Cohesion energy density: 0 J/m^3, volume flow rate: 0.05 μL/min, laser power: 265 mW, focal point from the bottom of the microchannel FD: 65 μm. The laser was irradiated during the initial 3 s and was turned off subsequently. This video corresponds to Figure 5b.

Movie S4. Video of the theoretical result for the light-induced assembly of microparticles using optical pressure in the microflow channel, where the interparticle binding force is strong. Cohesion energy density: 100 J/m^3, volume flow rate: 0.05 μL/min, laser power: 265 mW, focal point from the bottom of the microchannel FD: 65 μm. The laser was irradiated during the initial 3 s and was turned off subsequently. This video corresponds to Figure 5e.

Movie S5. Video of the theoretical result for the light-induced assembly of microparticles using optical pressure in the microflow channel, where there is no interparticle binding force. Cohesion energy density: 0 J/m^3, volume flow rate: 0.05μL/min, laser power: 265 mW, focal point from the bottom of the microchannel FD: 94 μm. The laser was irradiated during the initial 3 s and was turned off subsequently. This video corresponds to Figure 5c.

Movie S6. Video of the theoretical result for the light-induced assembly of microparticles using optical pressure in the microflow channel, where the interparticle binding force is strong. Cohesion energy density: 100 J/m^3, volume flow rate: 0.05 μL/min, laser power: 265 mW, focal point from the bottom of the microchannel FD: 94 μm. The laser was irradiated during the initial 3 s and was turned off subsequently. This video corresponds to Figure 5f.